Mon. Not. R. Astron. Soc. **000**, 000–000 (0000) Printed 1 February 2008 (MN LATEX style file v2.2)

Long-term X-ray variability and state transition of GX 339–4

A. K. H. Kong[1⋆], P. A. Charles[1,2], E. Kuulkers[3,4] and S. Kitamoto[5]
[1] *Department of Astrophysics, University of Oxford, Keble Road, Oxford OX1 3RH*
[2] *Department of Physics and Astronomy, University of Southampton, Southampton SO17 1BJ*
[3] *Space Research Organization Netherlands, Sorbonnelaan 2, 3584 CA Utrecht, the Netherlands*
[4] *Astronomical Institute, Utrecht University, P.O. Box 80000, 3507 TA Utrecht, the Netherlands*
[5] *Department of Physics, College of Science, Rikkyo University, 3-34-1, Nishi-Ikebukuro, Toshima-ku, Tokyo 171-8501, Japan*

Accepted. Received.

ABSTRACT

With extensive monitoring data spanning over 30 years from *Vela 5B*, *Ariel 5*, *Ginga*, *Compton Gamma Ray Observatory*, *Rossi X-ray Timing Explorer* and *BeppoSAX*, we find evidence for long-term X-ray variability on timescales $\sim$ 190–240 d from the black hole low-mass X-ray binary system GX 339–4. Such variability resembles the outburst cycle of Z Cam-type dwarf novae, in which the standard disc instability model plays a crucial role. If such a model is applicable to GX 339–4, then the observed variability might be due to the irradiation of an unstable accretion disc. We show that within the framework of the X-ray irradiation model, when the accretion rate exceeds a critical value, GX 339–4 enters a 'flat-topped' high/soft state, such as seen in 1998, which we suggest corresponds to the 'standstill' state of Z Cam systems.

Key words: accretion, accretion discs – binaries: close – black hole physics – stars: individual (GX 339–4) – X-rays: stars

1 INTRODUCTION

The black hole candidate GX 339–4 was discovered by Markert et al. (1973) with the *OSO-7* satellite and was soon noted for its similarity in X-ray behaviour to the classical black hole candidate Cyg X–1 (Markert et al. 1973; Maejima et al. 1984; Dolan et al. 1987). The source exhibits aperiodic and quasi-periodic modulations on time scales spanning milliseconds to years and over a wide range of wavelengths. Unlike typical soft X-ray transients (SXTs) which are barely detected in their quiescent state, GX 339–4 spends most of the time in the so-called X-ray low/hard state (LS) like a faint persistent source. During the LS, the energy spectrum can be described as a power-law with photon index of $\sim$ 1.5–2 (see Appendix for full list of references). It changes to the high/soft state (HS) occasionally (e.g. Maejima et al. 1984; Belloni et al. 1999) which are similar to the outbursts of transient sources. During the HS, it becomes brighter (in the 2–10 keV band) by a factor of $\sim$ 5–100 (see e.g. Kong et al. 2000, and references therein) and exhibits an ultra-soft spectral component plus a steeper power-law component. The 'low' and 'high' states referred to here are also called the 'hard' and 'soft' states so as to reflect the spectral behaviour. However, the luminosity of the 'low' state can sometimes be higher than the 'high' state (see Appendix) and hence it can be confusing to define the 'state' solely by the intensity of the X-rays. Therefore, a knowledge of the X-ray spectra are essential to distinguish different states accurately (see Table 1 of Kong et al. 2000 for the spectral and temporal properties of different states).

In addition to the LS and HS, GX 339–4 exhibits a very high state (VHS; Miyamoto et al. 1991) with a higher X-ray luminosity than in the HS (by a factor of $\sim$ 3). Note that the VHS also occurs in several other black hole soft X-ray transients (BHSXTs): GS 1124–683 (Ebisawa et al. 1994), XTE 1550–564 (Sobczak et al. 1999) and XTE J1748–288 (Revnivtsev, Trudolyubov & Borozdin 2000). An intermediate state (IS) in e.g. GX 339–4 (Méndez & van der Klis 1997) and 4U 1630–47 (Dieters et al. 2000) has also been reported and its spectral and timing properties are similar to the VHS but with a much lower luminosity. Finally, every now and then GX 339–4 enters an 'off' state (see Markert et al. 1973; Motch, Ilovaisky & Chevalier 1985; Ilovaisky et al. 1986; Asai et al. 1998; Kong et al. 2000), in which the

⋆ Present address: Harvard-Smithsonian Center for Astrophysics, 60 Garden Street, Cambridge, MA 02138, USA; Email: akong@cfa.harvard.edu

X-ray fast time variability and spectral shape are consistent with that seen in the LS (Méndez & van der Klis 1997), except that the 2–10 keV flux is at least ∼ 10 times lower than in the LS. It was concluded that the 'off' state is indeed an extension of the LS, but with lower luminosity (Kong et al. 2000; Corbel et al. 2000). It is worth noting that GX 339–4 and GS 1124–683 (Ebisawa et al. 1994) are the only X-ray sources observed in all these states; however, only GX 339–4 visits the different states so frequently (except for the VHS). We show in Figures 1–3 the different states of GX 339–4 in the past 30 years.

X-ray variability on long timescales (from days to years) has been found in many low-mass and high-mass X-ray binaries, but its origin is still an open question (e.g. Priedhorsky & Holt 1987; Schwarzenberg-Czerny 1992; Wijers & Pringle 1999; Ogilvie & Dubus 2001). Long-term X-ray variability has also been seen in the persistent black hole candidates Cyg X–1 (e.g. Kitamoto et al. 2000) and LMC X–3 (e.g. Paul, Kitamoto & Makino 2000). The timescales of their variability range from 100 days to 300 days. Given the similarity in X-ray properties between GX 339–4 and Cyg X–1, it is intriguing to investigate the long-term X-ray variability of GX 339–4. We therefore exploit the long-term capabilities of the all sky monitoring instruments on board the *Vela 5B*, *Ariel 5*, *Ginga*, *Compton Gamma Ray Observatory* and *Rossi X-ray Timing Explorer* to study the X-ray behaviour of this source on timescales of months to years.

2 LONG-TERM X-RAY OBSERVATIONS

GX 339–4 has been monitored by several X-ray missions in the last 30 years. We describe below all the instruments which contribute to the long-term X-ray light curves for this work. In addition, a new *BeppoSAX* observation of the source during the 'off' state is reported so that we can have a better understanding of the current status of the source. GX 339–4 has also been studied by other pointed observations which are summarised in the Appendix.

2.1 *Vela 5B*

The *Vela 5B* satellite (Conner, Evans & Belian 1969) monitored the X-ray sky from 1969 August to 1976 August (MJD 40367–43937) in two energy channels, 3–12 keV and 6–12 keV, the archival results of which are available from the High Energy Astrophysics Science Archive Research Center (HEASARC)[1]. The light curve (see Fig. 1) is made up from 508 data points using only the first channel (3–12 keV) since it has higher signal-to-noise ratio compared to the second channel (6–12 keV). Due to its limited temporal resolution and sensitivity, the data points exhibit a large scatter and only some outburst-like events were detected. It is interesting to note that there is a HS at ∼ MJD 41370 and 41660 (as indicated in Fig. 1) according to the pointed observations made by satellite *OSO-7* (Markert et al. 1973, see Appendix); however the intensity is not that high comparing to other data points.

[1] http://heasarc.gsfc.nasa.gov

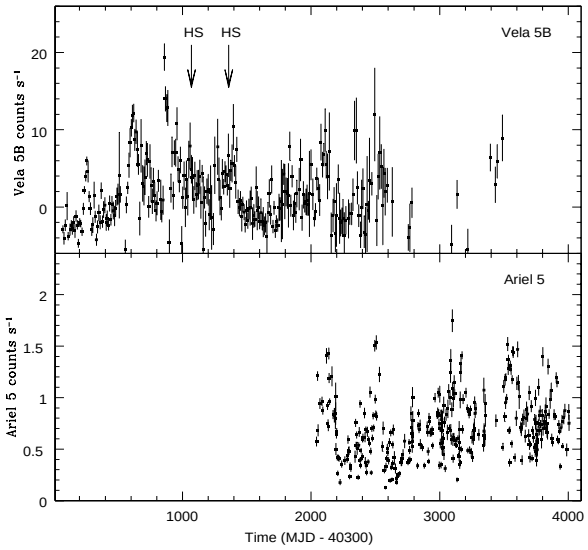

Figure 1. X-ray light curves of GX 339-4 as observed by: (upper panel) *Vela 5B* from 1969 – 1976. Arrows indicate the HS observed with *OSO-7*; (lower panel) *Ariel 5* ASM from 1974 – 1980. Both datasets were rebinned by a factor for 4 for clarity.

2.2 *Ariel 5*

The *Ariel 5* ASM experiment (Holt 1976) consisted of a pair of X-ray pinhole cameras with position sensitive proportional counters (3–6 keV) that covered 75% of the sky during each orbit (∼ 100 mins). From the archival HEASARC *Ariel 5* database, we obtained 2605 data points on GX 339–4 spanning the period from 1974 October to 1980 March (MJD 42338–44308; Fig. 1). Note that part of the *Ariel 5* data was collected simultaneously with the *Vela 5B* (see Fig. 1) and the count rate variations are consistent with each other. As for the *Vela 5B* data, the light curve shows considerable scatter as well as some clear flaring episodes. No pointed observations were carried out in this period and hence the X-ray 'state' of the source is not clear.

2.3 *Ginga* ASM

The *Ginga* ASM (Tsunemi et al. 1989) monitored the X-ray sky in the 1–20 keV band from 1987 February to 1991 October. The effective area of the *Ginga* ASM was about 420 cm^2 with a $45^\circ \times 1^\circ$ field-of-view. The sky-scanning observations were performed at intervals of a few days and covered about 70% of the sky. The typical exposure time for each scan across each observed source is about 3–18 s. During the observations from 1987 March to 1991 October (MJD 46860–48531), 215 data points were collected and it is very clear that four state transitions are seen in the light curve (Fig. 2), indicating excursions from the LS to the VHS/HS. The LS, HS and VHS state identifications were confirmed by the energy and power spectra obtained with the *Ginga* LAC (Miyamoto et al. 1991), *Granat* (Grebenev et al. 1993) and BATSE (Harmon et al. 1994) instruments. During the LS, the corresponding flux is always below 100 mCrab (1–6 keV) and in 1988 August (∼ MJD 47374), the source flux

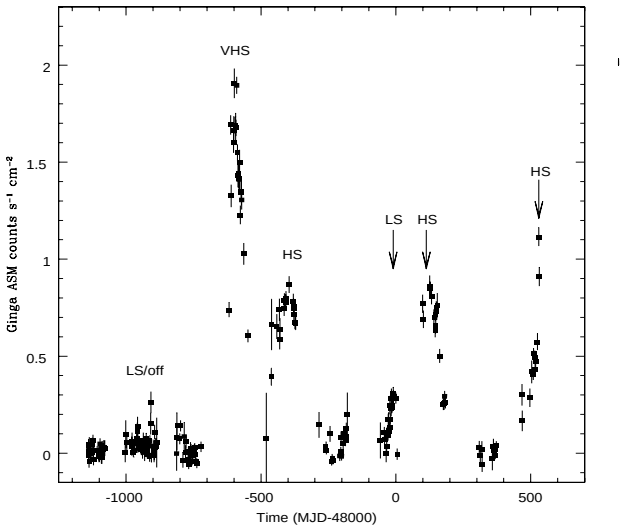

Figure 2. *Ginga* ASM 1–20 keV light curve of GX 339–4. This clearly shows that the source has gone through several different state transitions between 1987 and 1990. The arrows mark the time of *Granat* observations (see Appendix), which provide additional confirmation of the X-ray 'state'.

increased dramatically up to 1 Crab in ∼ 10 days. Subsequent *Ginga* LAC observations in 1988 September (∼ MJD 47405) revealed that the source was in a VHS. The flux then decreased to about 500 mCrab over ∼ 55 days, which presumably returned to the HS. By the end of 1989, the source again went to the LS until the other LS/HS transition between 1990 August and December (∼ MJD 48104–48226). The last LS/HS transition observed by *Ginga* took place in 1991 August which was observed simultaneously with BATSE and will be discussed in §2.5.

2.4 *RXTE* ASM

The All Sky Monitor (ASM; Levine et al. 1996) on board the *Rossi X-ray Timing Explorer* (*RXTE*; Bradt, Rothschild & Swank 1993) has monitored GX 339–4 several times daily in its 2–12 keV pass-band since 1996 February. The source remained at a low flux level (∼ 2 ASM cts/s or 27 mCrab) until early 1998 January (∼ MJD 50810) although some variations were seen (see inset of Fig. 3). Extensive pointed Proportional Counter Array (PCA) observations during this period indicate that it was in the LS (Wilms et al. 1999; Belloni et al. 1999). After MJD 50800, the source flux increased dramatically to ∼ 20 ASM cts/s (270 mCrab) where it stayed for about 200 days before declining. Belloni et al. (1999) reported that the source underwent a LS to HS transition, probably through an IS (∼ MJD 50820). The source changed back to the LS again in 1999 February (∼ MJD 51200). After 1999 June (∼ MJD 51330), the ASM count rate dropped further and the source intensity fell below the 3-σ detection level. Kong et al. (2000) found that the source entered the 'off' state at that time from *BeppoSAX* and optical observations. Note that the ASM count rate is also correlated with the hard X-rays as observed by BATSE (see next subsection). Interestingly, radio emission is also correlated with the X-ray during these different states (Fender et al. 1999; Corbel et al. 2000).

2.5 *CGRO* BATSE

The Burst and Transient Source Experiment (BATSE) on board the *Compton Gamma Ray Observatory (CGRO)* was operated continuously from April 5, 1991 (MJD 48351) until its re-entry on June 4, 2000 (MJD 51699). BATSE consists of eight identically configured detector modules with energy channels spanning from 20 to 600 keV (see Fishman et al. 1989). The GX 339–4 observations presented here were taken from the archival database which consists of data from 1991 April to 1999 August (MJD 48370–50554) in the 20–100 keV band. In constructing the light curve, the detector count rate is obtained by the Earth occultation technique (Harmon et al. 1994) and is fitted by an optically thin thermal bremsstrahlung (OTTB) model at a fixed temperature $kT = 60$ keV (Rubin et al. 1998), resulting in the photon fluxes presented here. The data presented in Fig.3 were rebinned by a factor of 2.

The BATSE light curve (see Fig. 3) shows about ten hard X-ray outbursts. The first hard X-ray outburst in 1991 August (∼ MJD 48470) was accompanied by *Ginga* ASM observations and two pointed observations by *Granat* (inset of Fig. 3). The soft and hard X-rays are more or less correlated until the hard X-rays reached maximum. The hard X-rays then decreased sharply and the source became very soft with a much steeper power law spectrum (Grebenev et al. 1993; Harmon et al. 1994); the source changed from the LS (as observed with the *Ginga* ASM) to the HS. The HS lasted for about 70 days, during which near-simultaneous radio data were available (Corbel et al. 2000) and then the source entered a possible 'off' state due to the non-detection of soft X-ray emission in the 3–10 keV band (Grebenev et al. 1993). The source then underwent three major hard X-ray outbursts before 1996 (MJD 50083) and a detailed energy spectral analysis of the BATSE data was presented by Harmon et al. (1994) and Rubin et al. (1998). In particular, the second one (MJD 49340–49420) is similar to the very first outburst (observed by *Ginga* observations), and radio observations (Corbel et al. 2000) suggest that the duration of the HS (after the sharp decrease in flux at ∼ MJD 49420) is also about 70 days. It is not clear whether there is a HS occurring between MJD 49000–49300 and MJD 49500–50100 since there is no soft X-ray and/or pointed data, but radio observations after MJD 49500 indicate that the source stayed in the LS (Corbel et al. 2000).

After the launch of *RXTE*, the source was monitored regularly by both the *RXTE*/ASM and BATSE and it is easily seen in the simultaneous light curves that the soft and hard X-rays are (anti) correlated in their gross behaviour, as already suggested from the simultaneous *Ginga* ASM and BATSE light curves. In addition, some 'mini'-outbursts with shorter recurrence times were also seen in the BATSE light curve. Extensive pointed *RXTE* observations suggest that the source was in the LS during these periods (Wilms et al. 1999; Belloni et al. 1999). BATSE initially observed three strong outbursts with near equal intensities and separations (∼ 400 days), the subsequent outbursts clearly show that the time between outbursts was variable, with a significant correlation between outburst fluence and time since the last

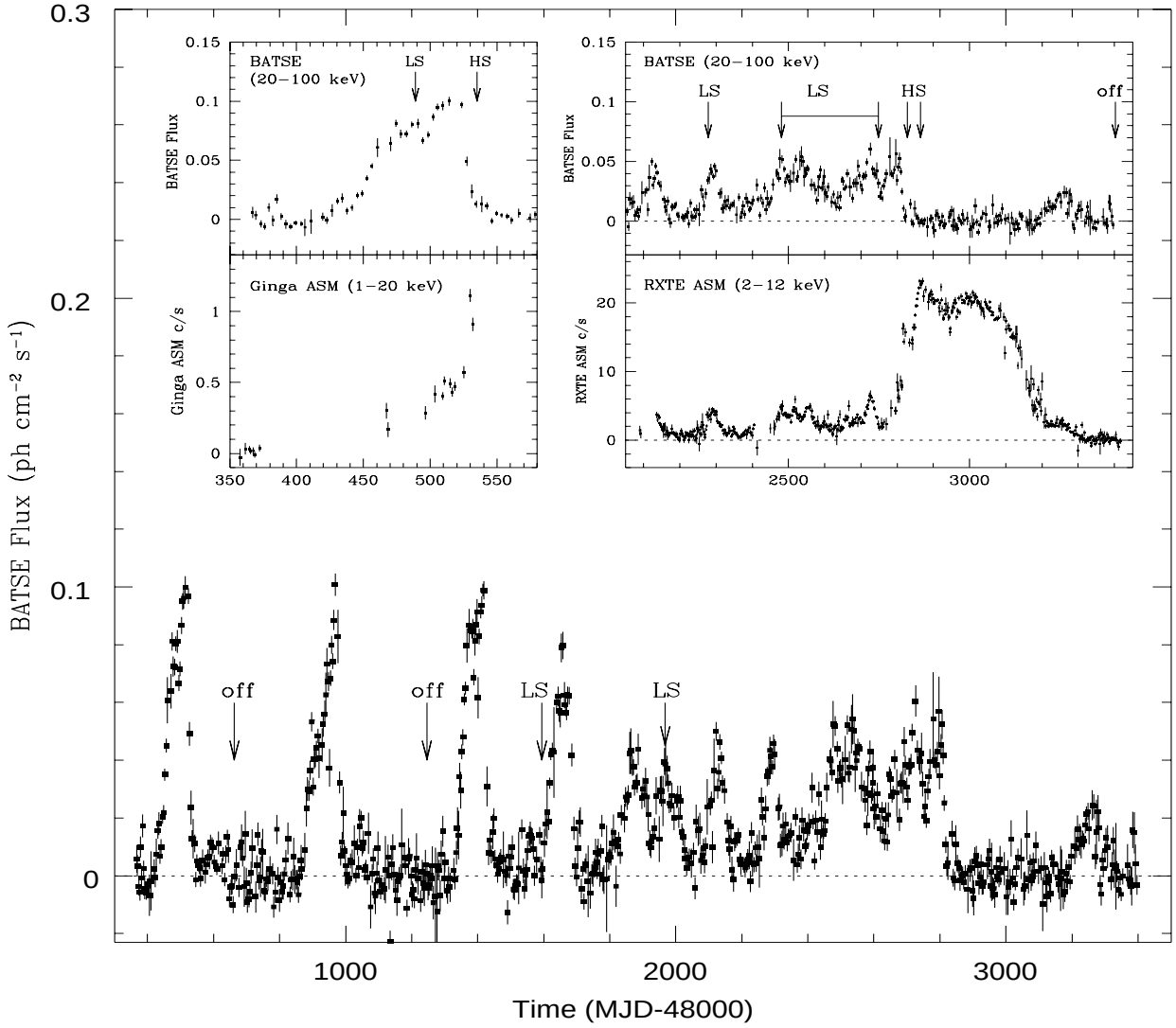

Figure 3. BATSE 20–100 keV light curve of GX 339–4 from 1991 – 1999. The data were rebinned by a factor of 2 for clarity. Also shown in the insets are the simultaneous BATSE and *Ginga* ASM light curves (left) and simultaneous BATSE and *RXTE* ASM light curves (right). The *RXTE* ASM data were rebinned by a factor of 2. Note that during a LS/HS transition, the BATSE flux drops to below the detection limit, while the soft X-rays (*Ginga* or *RXTE*) increase dramatically. The arrows mark the time of pointed observations (see Appendix) and the states are defined by the associated observations.

outburst (Rubin et al. 1998). The source changed from the LS to HS in 1998 January ($\sim$ MJD 50814) according to *RXTE* (ASM and PCA) observations (Belloni et al. 1999) and the BATSE flux dropped to below significant detection levels. Such a LS/HS transition was also accompanied by non-detection of radio emission (Corbel et al. 2000). The HS ended in 1999 February ($\sim$ MJD 51210) and the return to the LS was accompanied by the reappearance of the hard X-rays and radio emission (Corbel et al. 2000). Following the LS, the source entered the 'off' state (see §2.4) with a small drop in the BATSE flux.

2.6 *BeppoSAX*

We observed GX 339–4 with the Narrow Field Instruments (NFI) on board *BeppoSAX* between March 23.9 and 24.6, 2000 UT. The NFI consist of two co-aligned imaging instruments providing a field of view of $37' \times 57'$: the Low-Energy Concentrator Spectrometer (LECS; 0.1–10 keV; Parmar et al. 1997a) and the Medium Energy Concentrator Spectrometer (MECS; 1.6–10.5 keV; Boella et al. 1997). The other two NFI, non-imaging instruments are the Phoswich Detector System (PDS; 12–300keV; Frontera et al. 1997) and the High-Pressure Gas Scintillation Proportional Counter (HP–GSPC; 4–120 keV; Manzo et al. 1997).

Following the reduction procedures outlined by Kong et al. (2000), we applied an extraction radius of $4'$ centred on the source position for both LECS and MECS images

so as to obtain the source spectra. The MECS background was extracted by using long archival exposures on empty sky fields. For the LECS spectrum, we extracted the background from two semi-annuli in the same field of view as the source (see Parmar et al. 1999 for the reduction procedure). Both the extracted spectra were rebinned by a factor of 3 so as to accumulate at least 20 photons per bin and to sample the spectral full-width at half-maximum resolution (Fiore et al. 1999). A systematic error of 1% was added to both LECS and MECS spectra to take account of the systematic uncertainties in the detector calibrations (Guainazzi et al. 1998). Data were selected in the energy ranges 0.8–4.0 keV (LECS), 1.8–10.5 keV (MECS) and 15–220 keV (PDS) to ensure a better instrumental calibration (Fiore et al. 1999). A normalization factor was included for the LECS and PDS relative to the MECS in order to correct for the NFI's flux intercalibration (see Fiore et al. 1999).

The source was only detected in the 1–10 keV range, and the broad-band (1–10 keV) spectrum of GX 339–4 from the LECS and MECS data is satisfactorily ($\chi^2_\nu = 1.3$ for 33 degrees of freedom) fitted by a single power-law with photon index of 1.78 ± 0.24 plus absorption. We fixed the N_H at 5.1×10^{21} cm^{-2} (Kong et al. 2000). The absorbed flux in the 2–10 keV band is 0.69×10^{-12} erg cm^{-2}s^{-1}.

3 SEARCHING FOR X-RAY VARIABILITY ON LONG TIMESCALES

From the light curves shown in the above section, GX 339–4 underwent several state transitions and showed quasi-periodic variability in the past 30 years. We therefore exploit the data collected from different instruments to characterise its overall variability. In order to search for periodic phenomena, we used the Lomb-Scargle periodogram (Lomb 1976; Scargle 1982; hereafter LSP), a modification of the discrete Fourier transform which is generalised to the case of uneven spacing. We have also employed the Phase Dispersion Minimisation (PDM; Stellingwerf 1978) to check the results from the LSP, as the PDM is sensitive to non-sinusoidal modulations. For the *RXTE* ASM data (see inset of Fig. 3), we first excluded the most recent HS and 'off' state (after MJD 50815) from the dataset as the flat-topped HS will dominate the LSP and the data from the 'off' state are non-detection. By applying the LSP, a broad peak was found at periods around 190–240 d, centered at 213 d (see Fig. 4a). We also plot in Fig. 4a the 99% significance level for both white noise (Gaussian) and red noise. In determining the white-noise confidence level, we generate Gaussian noise datasets with the same time intervals and variance as the true data and then perform the LSP analysis on the resulting datasets. The peak power in each periodogram (which must be purely due to noise) was then recorded. This was repeated 10,000 times for good statistics. However, the noise is not necessarily Gaussian, it can also be frequency dependent with a higher power at lower frequencies. By using the above method, strong peaks at the low frequencies might give misleading results. In order to take into account such a noise contribution in the data, we simulate the noise as a power law, which is also known as red noise (e.g. Done et al. 1992). Quantitatively, the power spectrum of the red-noise light curve will be given by $(1/\omega)^\alpha$, where ω is frequency. Following an implementation of the method of Timmer & König (1995), we generate simulated light curves with the red-noise power spectrum, together with the same time sampling and mean variance as the original data. Finally, we combine the white-noise simulated light curve as mentioned above, with the red-noise simulated light curve, by scaling the data points in each such that the relative contribution of both white and red-noise components is matched with the real data. Following the method used previously to determine the white-noise confidence level, we derive the red-noise confidence level with the combined simulated light curve. Since red noise is frequency dependent, we need to compute the confidence level for a set of frequency bins. Hence it appears as a histogram rather than the continuous line for white-noise (see Fig. 4).

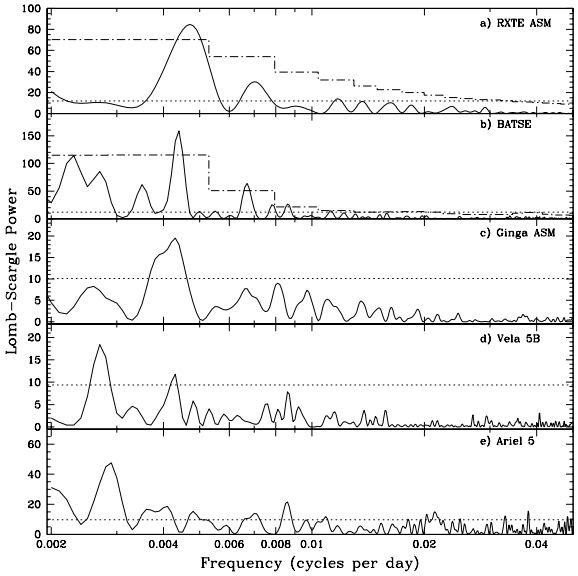

Figure 4. Lomb-Scargle periodograms of GX 339–4 as obtained by (a) *RXTE* ASM; (b) BATSE, (c) *Ginga* ASM, (d) *Vela 5B* and (e) *Ariel 5*, with significant peaks in the first four at 213, 227, 232 and 232d respectively. The horizontal dotted line is the 99% confidence level for white noise, while the dot-dash histogram is the 99% confidence level for red noise. The contribution of the red noise component in the *Ginga*, *Vela 5* and *Ariel 5* data is small enough ($\lesssim 1\%$) to be ignored since the noise level is essentially limited by the white noise.

The peak at 190–240 d is well above the 99% confidence levels (as determined by both methods) and we conclude that it is highly significant. The folded light curve of our *RXTE* ASM data on 228 d (which is consistent with the peaks in the *RXTE*, BATSE, *Ginga* and *Vela 5B* periodograms, and such that they are all on a common ephemeris for intercomparison of the structure so as to see whether the variability is stable) is shown in Fig. 5; T_0 is defined by the first data point of *Vela 5B*. Analysis with the PDM gave similar results to the LSP.

For the BATSE data, ten outbursts occurred during the past 7 years and like the *RXTE* ASM data, we exclude the recent high/soft and 'off' state (after MJD 50800) in calculating the LSP. The LSP shows a strong peak at 227±3 days

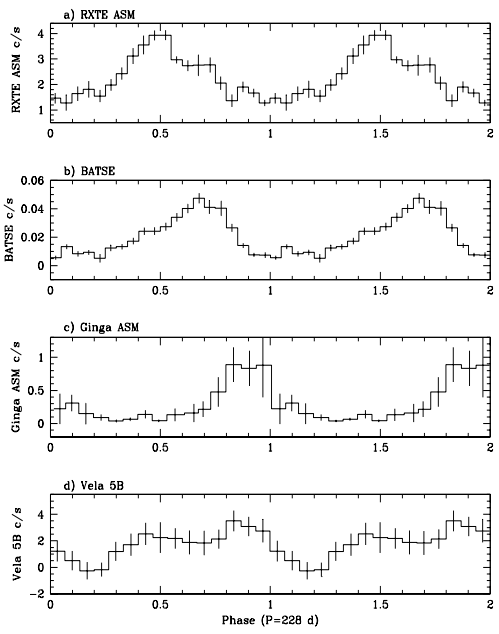

Figure 5. Folded light curves of *RXTE* ASM (a); BATSE (b), *Ginga* ASM (c) and *Vela 5B* (d) on a period of 228 d which is based on a common peak power determined in the LSP so that they are all on a common ephemeris for comparison of the structure. Two cycles are shown for clarity. T_0 is set at the time of the first data point of *Vela 5B*.

(Fig. 4b) which is consistent with the *RXTE* ASM result. The peak is very distinct and exceeds the 99% confidence level of both white and red noise. The PDM analysis also confirmed this modulation. The folded light curve of the BATSE data on 228 d is also shown in Fig. 5; T_0 is set at the time of the first data point of *Vela 5B*. We also tried to exclude the HS data at around MJD 48550 and 49450 (see §2.5) to calculate the LSP and the result was indistinguishable from those presented above.

The *Ginga* ASM monitored the source for 4.5 years and the four LS/HS/VHS state transitions on timescales of $\sim$ 200–400 d are seen (see Fig. 2). However, the sparse sampling prevents us from calculating a good LSP. Nevertheless, we include all the data points in searching for any variability. The strongest peak in the LSP is at $\sim$ 232 d, although it is broad and only marginally significant (see Fig.4c). The folded light curve of the *Ginga* data on 228 d is also shown in Fig. 5; T_0 is set at the time of the first data point of *Vela 5B*.

For the *Vela 5B* data, we used the whole dataset for calculating the LSP. It should be noted that two HS occurred during these observations (see Appendix; Markert et al. 1973) and hence the results should be interpreted with great caution. The strongest peak in the periodogram of the *Vela 5B* data is at $\sim$ 365 days and is caused by an annual variation in the spacecraft environment (Priedhorsky, Terrell & Holt 1983). The LSP reveals a second peak at 232 d which is just above the 99% confidence level (see Fig. 4d). Although the sensitivity of *Vela 5B* is poorer than current X-ray satellites, a clear variability is seen in the light curve (Fig. 1) and the long timebase (over 10 years) increases the sensitivity to these timescales. This variability was also detected in the PDM analysis. The folded light curve on 228 days is shown in Fig. 5; T_0 is again set at the time of the first data point of *Vela 5B*.

The *Ariel 5* ASM data do not show the variation as clearly as the *RXTE* ASM data, but some variability can be discerned. LS/HS transitions might occur during the *Ariel 5* observations but there is no pointed observations to confirm the 'state' of the source. We here used all the data in calculating the LSP. The LSP (Fig. 4e) shows a peak near 365 days, again due to the annual variation in the count rate from solar X-ray scattering or fluorescing from the Earth's atmosphere (Priedhorsky, Terrell & Holt 1983).

4 DISCUSSION

4.1 Long-term X-ray variability

Through the extensive dataset obtained with the *CGRO*/BATSE and *RXTE*/ASM, we find evidence of variability on timescales $\sim$ 190–240 d in GX 339–4 (it should be noted that the recent HS and 'off' state data are excluded in both datasets and at least one HS occurred in the BATSE data). Observations from *Ginga* and *Vela 5B* also suggest a similar timescale but the data consist of state transitions. Such a variability has been noted previously by Nowak, Wilms & Dove (1999) for the *RXTE* ASM data. They also pointed out that the observed long-term X-ray variability is not a strict clocking phenomenon but is more likely to be a characteristic timescale. From our analysis, this timescale is also manifested in the BATSE, *Ginga* and *Vela 5B* data.

In addition, the broad peak in the LSP of the *RXTE* ASM data (see Fig. 4) also hints that such variability is not strictly periodic and can only be regarded as a characteristic timescale. From the folded light curves of different datasets (Fig. 5), the peaks occur almost in anti-phase, suggesting the aperiodic nature. Indeed, such quasi-periodic long-term variability (usually referred to as the *super-orbital* period) has also been seen in other X-ray binaries such as Cyg X–2, LMC X–3 and Cyg X–1 (see e.g. Kong, Charles & Kuulkers 1998; Paul, Kitamoto & Makino 2000; Kitamoto et al. 2000), but no clear understanding of its origin has yet been established (see Wijers & Pringle 1999). As noted by Nowak, Wilms & Dove (1999), the observed long-term X-ray variability of GX 339–4 could be due to a combination of a quasi-steadily precessing disc at large radii with coronal structure changes on small radii. If this is the case, X-ray irradiation can give rise to a precessing disc (Dubus et al. 1999) and it might even explain the LS/HS transition of the source. Actually, results from the *Ginga* and *Vela 5B* data suggest that the LS/HS transitions and the outburst-like events during the low/hard state (as seen in the *RXTE* and BATSE data) may be due to the same mechanism, although the data is not well-sampled. Therefore, it is possible that such quasi-periodic outbursts might actually be a characteristic precursor to the LS/HS transition. In the next subsection, we will discuss the role of X-ray irradiation in the state transition and also the origin of the long-term X-ray variability.

Our *BeppoSAX* observations presented here indicate

that the source was fainter than the previous observation in 1999 August (see Kong et al. 2000) by a factor 3 in half year; therefore the source is still in the 'off' state. The energy spectra of both observations are very similar to those obtained in the LS. Hence, there is no doubt that the 'off' state is an extended LS (see discussions by Kong et al. 2000; Corbel et al. 2000) and we may now refine the source as a transient rather than a persistent source. In fact the luminosity during the 'off' state is in the upper end of the quiescent luminosity of typical X-ray transients (see e.g. Kong et al. 2000). The results also further confirm that during quiescence, significant X-ray variability can be seen. Such variability in quiescence is also found in several black hole transients such as GS 2023+338 (Wagner et al. 1994; Kong et al. 2001), 4U 1630–47 (Parmar et al. 1997b) and A0620–00 (Asai et al. 1998; Menou et al. 1999).

4.2 LS/HS transition in 1998

As noted in §2.4 and 2.5, GX 339–4 underwent a LS/HS transition in 1998 (see Fig. 3; also Belloni et al. 1999) which differs somewhat from the previous ones observed with the *Ginga* ASM. After the source reached the peak of the HS, it spent nearly 200 days at a constant flux level of ~ 20 *RXTE*/ASM cts/s. Such a flat-topped X-ray light curve for GX 339–4 is different from the 'standard' fast-rise exponential decay profile, as observed from various X-ray transients (see Chen, Shrader & Livio 1997 for various examples of different outburst patterns). The state transition mechanism for such a persistent source is still a puzzle and observations in different states suggested that it is most likely associated with the mass accretion rate (e.g. Méndez & van der Klis 1997). A change in the mass accretion rate can be caused by a thermal instability in the accretion disc (disc instability model, or DIM) and in fact it is widely accepted that the outbursts in BHSXTs are due to this mechanism (e.g. Esin, Lasota & Hynes 2000). Interestingly, the DIM was originally developed to describe the outbursts in dwarf novae (DN; see e.g. Cannizzo 1993 for a review) which contain a white dwarf as the compact object; it was suggested quite early that it also applies in BHSXTs (e.g. van Paradijs & Verbunt 1984; Huang & Wheeler 1989; Mineshige & Wheeler 1989). In LMXBs, X-ray irradiation can influence the stability of the accretion disc (van Paradijs 1996) and thus a DIM which includes X-ray irradiation was developed (Dubus et al. 1999). It is worth noting that the recent HS spectroscopic observations of GX 339–4 obtained by Wu et al. (2001) also indicate that the accretion disc is heated by soft X-ray irradiation, suggesting that irradiation plays a role in the state transition. Irradiation of the outer disc by X-rays from the inner disc gives a stability criterion, from which the minimum mass accretion rate for a stable, steady-state accretion in an X-ray irradiated disc can be expressed as (Dubus et al. 1999):

$$\dot{M}_{crit}^{irr} \approx 2.0\times10^{15}\left(\frac{M_1}{M_\odot}\right)^{0.5}\left(\frac{M_2}{M_\odot}\right)^{-0.2}\times P_{hr}^{1.4}\left(\frac{\mathcal{C}}{5\times10^{-4}}\right)^{-0.5}\ \mathrm{g\ s^{-1}}, \quad (1)$$

where M_1 is the black hole mass, M_2 is the mass of the companion, P_{orb} the orbital period in hours. $\mathcal{C}$ is a parameter to describe the properties of irradiation through:

$$T_{irr}^4 = \mathcal{C}\frac{\dot{M}c^2}{4\pi\sigma R^2}, \quad (2)$$

where T_{irr} is the irradiation temperature and σ is the Stefan-Boltzmann constant. For a stable X-ray irradiated disc during the HS, $\dot{M}_{crit}^{irr}$ can be estimated from the HS observations by Belloni et al. (1999), in which they have fitted the spectrum with a power law plus a multi-colour disc blackbody model. By using the derived inner disc radius, $R_{in}\sqrt{\cos i}$ of $25.4D_4$ km (where D_4 is the distance to the source in units of 4 kpc; Zdziarski et al. 1998) and the blackbody temperature, T_{in} of 0.72 keV, we can calculate the bolometric luminosity of the disc blackbody component as

$$\begin{aligned} L_X &= 4\pi R_{in}^2\sigma T_{in}^4 \\ &= 2.2\times10^{37}D_4^2/\cos i \quad \mathrm{erg\ s^{-1}}. \end{aligned} \quad (3)$$

The accretion rate can be estimated via the relation $L_X = 0.5GM_1\,\dot{M}/R_{in}$, which leads to $\dot{M} \approx 1.7\times10^{17}D_4^2$ g s^{-1} if we assume an orbital inclination of about 15° (Wu et al. 2001) for a 14.8-hr orbital period (Callanan et al. 1992). Assuming an estimated mass of the black hole of $5\,M_\odot$ (Zdziarski et al. 1998) and companion star of $0.4\,M_\odot$ (Callanan et al. 1992), we obtain $\mathcal{C} = 9.4\times10^{-4}$ from Eqn. 1, which is slightly higher than 5×10^{-4} obtained by comparison with other results in the literature (see Dubus et al. 1999). According to the scenario outlined above, the mass of the compact object is limited to be ~ 3–$5\,M_\odot$.

From the previous LS observations, the estimated mass accretion rate is about 5×10^{16} g s^{-1} (e.g. Wilms et al. 1999; Belloni et al. 1999) which is a factor of 3 below the critical accretion rate for a stable disc and hence the disc may be subject to the DIM in order to give rise to a LS/HS transition. Since the accretion rate during the LS is very close to the critical value, a slight increase in the accretion rate by a small factor would produce a stable disc. As a result, a shorter interval to the next state transition would be expected. Unlike the SXTs in which the outburst timescale is normally longer than ten years, GX 339–4 has much more frequent state transitions, as seen in e.g. the *Ginga* ASM data (see Fig. 2). In fact, the 232-d variability seen in the *Ginga* and *Vela 5B* data has already hinted at such behaviour.

The most interesting behaviour of the 1998 HS is that the observed flat-topped X-ray light curve of GX 339–4 bears characteristics of Z Cam-type DN in which standstills (i.e. the brightness remains constant) occasionally interrupt the recurrent outbursts. Such a scenario can be explained by the DIM (Meyer & Meyer-Hofmeister 1983; King & Cannizzo 1998) in which the accretion rate before standstill is very close to a critical value and a sudden increase in the accretion rate (e.g. by a starspot or irradiation induced mass overflow) triggers the standstill state. The light curve of GX 339–4 is even more similar to the model proposed by King & Cannizzo (1998) in which the standstill is at a higher luminosity than the normal outbursts. For Z Cam systems, the intensity of the standstills is lower than the maximum of the outbursts (Meyer & Meyer-Hofmeister 1983), but we should note that

the models for explaining the Z Cam systems are used to account for optical light curves.

The second similarity between GX 339–4 and Z Cam systems concerns the recurrence of outbursts between standstills. From our earlier period analysis of the archival GX 339–4 data over 30 years, we find a variability timescale of ∼190–240 d and we suggest this to be the recurrent outbursting behaviour seen in Z Cam systems. As pointed out by Dubus et al. (in preparation), the accretion rate can vary on timescales of 10–100 days when a viscously unstable disc is irradiated by a constant X-ray flux. If irradiation is crucial for determining the accretion rate of GX 339–4, this may explain the variability of the 'mini'-outbursts observed during the LS. There is also an indication that the accretion rate of GX 339–4 was building up before the HS in 1998 as the average intensity level of both *RXTE* ASM and BATSE data has a slight increasing trend especially after MJD 50000 (see Fig. 3). In addition, the HS occurring at MJD 48550 and 49450 (see §2.5) were just after a strong X-ray outburst in the LS (see Fig. 3). Perhaps this takes the accretion rate in the LS to be close to the critical value and finally triggers the state transition. As a result, this HS may be simply a strong, prolonged outburst in an otherwise LS. In fact, from the period analysis of the *Vela 5B* and *Ginga* data for which state transitions are included in the calculation, the timescale of variability resembles that found in the *RXTE* ASM data in the LS. Perhaps the LS outbursts may be excursions towards the HS but which they do not quite reach. If this is the case, we would expect similar spectral evolution during the LS outburst, just like during a state transition. However, such outbursts are usually short and therefore observations are difficult to arrange. The most likely observations available are from Wilms et al. (1999), in which an *RXTE* pointed observation of GX 339–4 was made near the outburst (MJD 50710) just before the LS/HS transition. Although the energy spectrum appeared to be slightly softer, it is still consistent with other LS observations within the uncertainties. It is worth noting that Cyg X–1 also shows LS/HS transitions occasionally and it has flaring activities during the LS. Moreover, the long HS of Cyg X–1 between 1996 May and August resembles that seen in GX 339–4, but with more flares during the HS (Zhang et al. 1997). Therefore, it is possible that the state transition of Cyg X–1 is due to a similar mechanism to that discussed here (see however Zhang et al. 1997; Esin et al. 1998). More recently, LMC X–3 was also shown to have recurring state transitions but the driving force is very likely to be due to other mechanisms (Boyd et al. 2000; Wilms et al. 2001). Given that the accretion rate in the LS is close to the critical value, similar LS/HS transitions would be expected in the near future and multi-wavelength observations of such transitions, particularly the correlation between the X-ray, optical and radio emissions will constrain the accretion disc structure and behaviour of the secondary star.

ACKNOWLEDGMENTS

We are grateful to Colleen Wilson-Hodge and Ken Watanabe for providing the updated BATSE data. We also thank Christine Done for the red-noise generator code. AKHK is supported by a Hong Kong Oxford Scholarship. This paper utilizies quick-look results provided by the ASM/RXTE team and data obtained through the HEASARC Online Services of NASA/GSFC.

APPENDIX A: PREVIOUS POINTED X-RAY OBSERVATIONS OF GX 339–4

GX 339–4 has been observed by several X-ray satellites in the past 30 years and the results from those pointed observations are crucial to determine the 'state' of the source. We compile here a list of pointed observations of GX 339–4 from the literature (see Table A1). Note that the 'state' quoted is determined by spectral and temporal analysis. Although the X-ray flux level can more or less reflect the 'state' of the source, on several occasions the X-ray flux in the LS is actually higher than the HS (e.g. 1981 May and 1984 May). Hence the X-ray intensity itself is not an accurate indicator of X-ray 'state'.

Table A1. Previous X-ray observations of GX 339–4.

Date	X-ray state	Flux (mCrab)	Satellite	References
1971 October to 1972 January	LS	$\sim$ 10–40 (1–6 keV)	*OSO-7*	1
1972 February	HS	$\sim$ 90 (1–6 keV)	*OSO-7*	1
1972 May	LS/off	$<$ 5 (1–6 keV)	*OSO-7*	1
1972 December	HS	$\sim$ 300 (1–6 keV)	*OSO-7*	1
1981 March	LS/off	$<$ 30	*Hakucho*	2
1981 May	LS	160 (0.1–20 keV)	*Hakucho*	2, 3
1981 June	LS to HS	$\sim$ 160–600 (3–6 keV)	*Hakucho*	2
1982 May	LS/off	$<$ 15	*Hakucho*	2
1983 May	HS	300 (2–10 keV)	*Tenma*	4
1984 March & May	IS	90 (2–10 keV)	*EXOSAT*	5
1984 May	HS	120 (0.1–20 keV)	*EXOSAT*	3
1985 April	LS/off	1.7 (0.1–20 keV)	*EXOSAT*	3
1987 June	LS/off	$\sim$ 13 (1–6 keV)	*Ginga*	6, 7
1987 July	LS/off	$\sim$ 26 (1–6 keV)	*Ginga*	6, 7
1988 September	VHS	900 (1–6 keV)	*Ginga*	7, 8
1989 August	LS/off	$\sim$ 12 (1–6 keV)	*Ginga*	7, 9
1990 April	LS	100 (3–10 keV)	*Granat*	10
1990 August	HS	100–230 (3–10 keV)	*Granat*	10
1991 February	off	$<$ 6 (3–10 keV)	*Granat*	10
1991 August to October	LS to HS	$\sim$ 100–300 (3–10 keV)	*Granat*	10
1992 February	off	$<$ 17 (3–10 keV)	*Granat*	10
1993 September	off	$<$ 0.01 (2–10 keV)	*ASCA*	11
1994 August	LS	$\sim$ 30 (3–9 keV)	*ASCA*	12
1995 September	LS	50 (3–9 keV)	*ASCA*	12
1996 July	LS	70 (2–12 keV)	*RXTE*	13
1997 February to October	LS	$\sim$ 70 (2–12 keV)	*RXTE*	12
1998 January to February	HS	160–270 (2–12 keV)	*RXTE*	13
1998 August	HS	260 (2–12 keV)	*RXTE*	14
1999 August	off	0.1 (2–10 keV)	*BeppoSAX*	14, 15
2000 March	off	0.03 (2–10 keV)	*BeppoSAX*	this work

References: (1) Markert et al. 1973; (2) Motch et al. 1985; (3) Ilovaisky et al. 1986; (4) Makishima et al. 1986; (5) Méndez & van der Klis 1997; (6) Callanan et al. 1992; (7) Kitamoto et al. 1992; (8) Miyamoto et al. 1991; (9) Steiman-Cameron et al. 1990; (10) Grebenev et al. 1993; (11) Asai et al. 1998; (12) Wilms et al. 1999; (13) Belloni et al. 1999; (14) Corbel et al. 2000; (15) Kong et al. 2000

REFERENCES

Asai K., Dotani T., Hoshi R., Tanaka Y., Robinson C. R., Terada K., 1998, PASJ, 50, 611.

Belloni T., Méndez M., van der Klis M., Lewin W. H. G., Dieters S., 1999, ApJ, 519, L159.

Boella G., Butler R.C., Perola G.C., Piro L., Scarsi L., Bleeker J.A.M., 1997, A&AS, 122, 299.

Boyd P. T., Smale A. P., Homan J., Jonker P. G., van der Klis M., Kuulkers E., 2000 ApJ, 542, L127.

Bradt H. V., Rothschild R. E., Swank J. H., 1993, ApJSS, 97, 355.

Callanan P. J., Charles P. A., Honey W. B., Thorstensen J. R., 1992, MNRAS, 259, 395.

Cannizzo J., 1993, In: *Accretion Disks in Compact Stellar Systems*, p. 6, ed. Wheeler J., World Scientific, Singapore.

Chen W., Shrader C. R., Livio M., 1997, ApJ, 491, 312.

Conner J. P., Evans W. D., Belian R. D., 1969, ApJ, 157, L157.

Corbel S., Fender R. P., Tzioumis A. K., McIntyre V., Nowak M., Durouchoux P., Sood R., 2000, A&A, 359, 251

Dieters S. W. et al., 2000, ApJ, 538, 307.

Dolan J. F., Crannell C. J., Bennis B. R., Orwig L. E., 1987, ApJ, 322, 324.

Done C., Madejski G. M., Mushotzky R. F., Turner T. J., Koyama K., Kunieda H., 1992, ApJ, 400, 138.

Dubus G., Lasota J. P., Hameury J. M., Charles P., 1999, MNRAS, 303, 139.

Ebisawa K., Ogawa M., Aoki T., Dotani T., Takizawa M., Tanaka Y., Yoshida K., 1994, PASJ, 46, 375.

Esin A. A., Lasota, J.-P., Hynes, R. I., 2000, A&A, 354, 987.

Esin A. A., Narayan R., Cui W., Grove J. C., Zhang S. N., 1998, ApJ, 505, 854.

Fender R. et al., 1999, ApJ, 519, L165.

Fiore F., Guainazzi M., Grandi P., 1999, Cookbook for BeppoSAX NFI Spectral Analysis, Version 1.2.

Fishman G. J. et al., 1989, In: *Proc. of the GRO Science Workshop*, p. 2, ed. Johnson W. N., NASA/GSFC, Greenbelt.

Frontera F., et al., 1997, A&AS, 122, 357.

Grebenev S. et al., 1993, A&ASS, 97, 281.

Harmon B. A. et al., 1994, ApJ, 425, L17.

Holt S. S., 1976. Ap&SS, 42, 123.

Huang M., Wheeler J. C., 1989, ApJ, 343, 229

Ilovaisky S. A., Chevalier C., Motch C., Chiappetti L., 1986, A&A, 164, 67.

King A. R., Cannizzo J. K., 1998, ApJ, 499, 348.

Kitamoto S., Egoshi W., Miyamoto S., Tsunemi H., Ling J., Wheaton W. A., Paul B., 2000, ApJ, 531, 546.

Kitamoto S., Miyamoto S., Tsunemi H., Hayashida K., 1992, In: Frontiers of X-ray Astronomy, p. 321, eds Tanaka Y., Nomoto K., Universal Academy Press, Inc., Tokyo, Japan.

Kong A. K. H., Charles P. A., Kuulkers E., 1998, New Astronomy, 3, 301.

Kong A. K. H., Kuulkers E., Charles P. A., Homer L., 2000, MNRAS, 312, L49.

Kong A. K. H., McClintock J. E., Garcia M. R., Murray S. S., Barret D., 2001, ApJ, submitted

Levine A. M., Bradt H. V., Cui W., Jernigan J. G., Morgan E. H., Remillard R., Shirley R. E., Smith D. A., 1996, ApJ, 469, L33.

Maejima Y., Makishima K., Matsuoka M., Ogawara Y., Oda M., Tawara Y., Doi K., 1984, ApJ, 285, 712.

Makishima K., Maejima Y., Mitsuda K., Bradt H. V., Remillard R. A., Touhy I. R., Hoshi R., Nakagawa M., 1986, ApJ, 308, 635.

Manzo G., et al., 1997, A&AS, 122, 341.

Markert T. H., Canizares C. R., Clark G. W., Lewin W. H. G., Schnopper H. W., Sprott G. F., 1973, ApJ, 184, L67.

Méndez M., van der Klis M., 1997, ApJ, 479, 926.

Menou K., Esin A. A., Narayan R., Garcia M. R., Lasota J.-P., McClintock, J. C., 1999, ApJ, 520, 276.

Meyer F., Meyer-Hofmeister E., 1983, A&A, 121, 29.

Mineshige S., Wheeler J. C., 1989, ApJ, 343, 241

Miyamoto S., Kimura K., Kitamoto S., Dotani T., Ebisawa K., 1991, ApJ, 383, 784.

Motch C., Ilovaisky S. A., Chevalier C., 1985, Sp. Sci. Rev., 40, 219.

Nowak M. A., Wilms J., Dove J., 1999, ApJ, 517, 355.

Ogilvie G. I., Dubus G., 2001, MNRAS, 320, 485.

Parmar A.N., et al., 1997a, A&AS, 122, 309.

Parmar A.N., Oosterbroek Y., Orr A., Guainazzi M., Shane N., Freyberg M.J., Ricci D., Malizia A., 1999, A&AS, 139, 407.

Parmar A. N., Williams O. R., Kuulkers E., Angelini L., White N. E., 1997b, A&A, 319, 855.

Paul B., Kitamoto S., Makino F., 2000, ApJ, 528, 410.

Priedhorsky W. C., Holt S. S., 1987, Sp. Sci. Rev., 45, 291.

Priedhorsky W. C., Terrell J., Holt S. S., 1983, ApJ, 270, 233.

Revnivtsev M. G., Trudolyubov S. P., Borozdin K. N., 2000, MNRAS, 312, 151.

Rubin B. C., Harmon B. A., Paciesas W. S., Robinson C. R., Zhang S. N., Fidhman G. J., 1998, ApJ, 492, L67.

Schwarzenberg-Czerny A., 1992, A&A, 260, 268.

Sobczak G. J., McClintock J. E., Remillard R. A., Levine A. M., Morgan E. H., Bailyn C. D., Orosz J. A., 1999, ApJ, 517, L121.

Steiman-Cameron T., Imamura J., Middleditch J., Kristian J., 1990, ApJ, 359, 197.

Stellingwerf R. F., 1978, ApJ, 224, 953.

Timmer J., König M., 1995, A&A, 300, 707.

Tsunemi H., Kitamoto S., Makoto M., Miyamoto S., Yamashita K., 1989, PASJ, 41, 391.

van Paradijs J., 1996, ApJ, 464, L139.

van Paradijs J., Verbunt F., 1984, in AIP Conf. Proc. 115, High-Ebergy Transients in Astrophysics, ed. S. E. Woosley (New York: AIP), 49

Wagners R. M., Starrfield S. G., Hjellming R. M., Howell S. B., Kreidl T. J., 1994, ApJ, 429, L25.

Wijers A. M. J., Pringle J. E., 1999, MNRAS, 308, 207.

Wilms J., Nowak M. A., Dove J. B., Fender R. P., Di Matteo T., 1999, ApJ, 522, 460.

Wilms J., Nowak M. A., Pottschmidt K., Heindl W. A., Dove J. B., Begelman M. C., 2001, MNRAS, 320, 327.

Wu K., Saria R., Hunstead W., Johnston H. M. 2001, MNRAS, 320, 177.

Zhang S. N., Cui W., Harmon B. A., Paciesas W. S., Remillard R. E., van Paradijs J., 1997, ApJ, 477, L95.

Zdziarski A., Andrzej A., Poutanen J., Mikolajewska J., Gierlinski M., Ebisawa K., Johnson W. N., 1998, MNRAS, 301, 435.